Combining First and Second Order Continuity Constraints in Ultrasound Elastography

Md Ashikuzzaman, *Student Member, IEEE*, Ali Sadeghi-Naini, *Senior Member, IEEE*, Abbas Samani, *Senior Member, IEEE* and Hassan Rivaz, *Senior Member, IEEE*

APPENDIX

In this Appendix, we explain matrices H, H_1, D, D_2 and vectors μ and b_s.

$H \in \mathbb{R}^{2mn \times 2mn}$ is a symmetric tridiagonal matrix: $H = diag(h^{'2}(1,1), h^{'2}(1,2), .., h^{'2}(m,n))$ where $h^{'2}(i,j)$ is defined by:

$$h^{'2}(i,j) = \begin{bmatrix} I_{2,a}^{'2}(i,j) & I_{2,a}^{'}(i,j)I_{2,l}^{'}(i,j) \\ I_{2,a}^{'}(i,j)I_{2,l}^{'}(i,j) & I_{2,l}^{'2}(i,j) \end{bmatrix} \quad (1)$$

where $I_{2,a}^{'}(i,j)$ and $I_{2,l}^{'}(i,j)$ denote the axial and lateral derivatives of I_2 at point $(i + a_{i,j}, j + l_{i,j})$. $H_1 \in \mathbb{R}^{2mn \times 2mn}$ is a diagonal matrix defined as: $H_1 = diag(I_{2,a}^{'}(1,1), I_{2,l}^{'}(1,1), I_{2,a}^{'}(1,2), I_{2,l}^{'}(1,2), \ldots, I_{2,a}^{'}(m,n), I_{2,l}^{'}(m,n))$. $\mu \in \mathbb{R}^{2mn \times 1}$ is defined as:

$$\mu = \begin{bmatrix} g_{1,1}, g_{1,1}, g_{1,2}, g_{1,2}, \ldots, g_{m,n} \end{bmatrix}^T \quad (2)$$

where

$$g_{i,j} = I_1(i,j) - I_2(i + a_{i,j}, j + l_{i,j}) \quad (3)$$

$D \in \mathbb{R}^{2mn \times 2mn}$ is a sparse block matrix which contains the regularization parameters stemming from optimization of the first-order continuity term R_1. Note that the matrix D of this work is exactly the same as that of GLUE. Therefore, we show D in Section I of the Supplementary Material. D_2 is a sparse matrix of size $2mn \times 2mn$ which is defined as follows:

$$D_2 = \begin{bmatrix} Q^{'} + \Gamma & R_1^{'} & R_2^{'} & O & \ldots & \ldots & \ldots & O \\ R_1^{'} & Q^{''} & R_1^{''} & R_2^{'} & \ddots & \ddots & \ddots & \vdots \\ R_2^{'} & R_1^{''} & S^{'} & R_1^{''} & \ddots & \ddots & \ddots & \vdots \\ O & R_2^{'} & R_1^{''} & S^{'} & \ddots & \ddots & \ddots & \vdots \\ \vdots & \ddots & \ddots & \ddots & \ddots & \ddots & \ddots & O \\ \vdots & \ddots & \ddots & \ddots & \ddots & S^{'} & R_1^{''} & R_2^{'} \\ \vdots & \ddots & \ddots & \ddots & \ddots & R_1^{''} & Q^{''} & R_1^{'} \\ O & \ddots & \ddots & \ddots & O & R_2^{'} & R_1^{'} & Q^{'} \end{bmatrix} \quad (4)$$

where O is a zero matrix of size $2n \times 2n$. $R_1^{'}$, $R_1^{''}$ and $R_2^{'}$ are diagonal matrices of size $2n \times 2n$ and defined as: $R_1^{'} = diag(-2\theta_1, -2\lambda_1, ..., -2\theta_1, -2\lambda_1)$, $R_1^{''} = diag(-4\theta_1, -4\lambda_1, ..., -4\theta_1, -4\lambda_1)$ and $R_2^{'} = diag(\theta_1, \lambda_1, ..., \theta_1, \lambda_1)$.

Γ is a diagonal matrix of size $2n \times 2n$ which is defined as $\Gamma = diag(\gamma, 0, \gamma, 0, ..., \gamma, 0)$. $b_s \in \mathbb{R}^{2mn \times 1}$ is the adaptive regularization term and defined as:

$$b_s = \begin{bmatrix} b_{init} & b_{mid} & \ldots & b_{mid} & b_{end} \end{bmatrix}^T \quad (5)$$

b_{init}, b_{mid} and b_{end} are vectors of size $2n$ and defined in Eqs. 6, 7 and 8, respectively.

$$b_{init} = \begin{bmatrix} -(\alpha_1 + \alpha_2)\epsilon_a, -(\beta_1 + \beta_2)\epsilon_l, -\alpha_1\epsilon_a, -\beta_1\epsilon_l, \ldots, \\ -\alpha_1\epsilon_a, -\beta_1\epsilon_l, -\alpha_1\epsilon_a + \alpha_2\epsilon_a, -\beta_1\epsilon_l + \beta_2\epsilon_l \end{bmatrix} \quad (6)$$

$$b_{mid} = \begin{bmatrix} -\alpha_2\epsilon_a & -\beta_2\epsilon_l & 0 & \ldots & 0 & \alpha_2\epsilon_a & \beta_2\epsilon_l \end{bmatrix} \quad (7)$$

$$b_{end} = \begin{bmatrix} (\alpha_1 - \alpha_2)\epsilon_a, (\beta_1 - \beta_2)\epsilon_l, \alpha_1\epsilon_a, \beta_1\epsilon_l, \ldots, \\ \alpha_1\epsilon_a, \beta_1\epsilon_l, \alpha_1\epsilon_a + \alpha_2\epsilon_a, \beta_1\epsilon_l + \beta_2\epsilon_l \end{bmatrix} \quad (8)$$

$Q^{'}$, $Q^{''}$ and $S^{'}$ have been defined in Section I of the Supplementary Material.

Combining First and Second Order Continuity Constraints in Ultrasound Elastography

Md Ashikuzzaman, *Student Member, IEEE*, Ali Sadeghi-Naini, *Senior Member, IEEE*, Abbas Samani, *Senior Member, IEEE* and Hassan Rivaz, *Senior Member, IEEE*

This Supplementary Material presents the matrices D, $Q^{'}$, $Q^{''}$ and $S^{'}$. In addition, we report GLUE strain images using strong weights. Besides, we analyze the effect of a 50% increase in continuity weights on SOUL strain. Moreover, we demonstrate the impact of regularizing the first sample on strain estimates. Furthermore, we investigate the correlation between pixel size and regularization parameter values. We also show the strain images corresponding to different realizations of the simulated layer phantom. Finally, we report the lateral strain images obtained by GLUE and SOUL.

matrix of size $2n \times 2n$. Q and S are matrices of size $2n \times 2n$ and defined by Eqs. 2 and 3.

$Q^{'}$, $Q^{''}$ and $S^{'}$ are sparse matrices of size $2n \times 2n$ and defined as Eqs. 4, 5 and 6, respectively.

I. METHODS

$D \in \mathbb{R}^{2mn \times 2mn}$ is defined in Eq. 1.

$$D = \begin{bmatrix} Q & R & O & O & \dots & O \\ R & S & R & O & \dots & O \\ O & R & S & R & \dots & O \\ \vdots & & \ddots & \ddots & \ddots & \\ O & O & \dots & R & S & R \\ O & O & \dots & O & R & Q \end{bmatrix} \quad (1)$$

where $R = diag(-\alpha_1, -\beta_1, ..., -\alpha_1, -\beta_1)$. O is a zero

$$Q = \begin{bmatrix} \alpha_1 + \alpha_2 & 0 & -\alpha_2 & 0 & 0 & \dots & 0 \\ 0 & \beta_1 + \beta_2 & 0 & -\beta_2 & 0 & \dots & 0 \\ -\alpha_2 & 0 & \alpha_1 + 2\alpha_2 & 0 & -\alpha_2 & \dots & 0 \\ 0 & -\beta_2 & 0 & \beta_1 + 2\beta_2 & 0 & \dots & 0 \\ 0 & 0 & -\alpha_2 & 0 & \alpha_1 + 2\alpha_2 & \dots & 0 \\ \vdots & & & & & \ddots & \\ 0 & 0 & 0 & \dots & & \alpha_1 + \alpha_2 & 0 \\ 0 & 0 & 0 & \dots & & 0 & \beta_1 + \beta_2 \end{bmatrix} \quad (2)$$

$$S = \begin{bmatrix} 2\alpha_1 + \alpha_2 & 0 & -\alpha_2 & 0 & 0 & \dots & 0 \\ 0 & 2\beta_1 + \beta_2 & 0 & -\beta_2 & 0 & \dots & 0 \\ -\alpha_2 & 0 & 2\alpha_1 + 2\alpha_2 & 0 & -\alpha_2 & \dots & 0 \\ 0 & -\beta_2 & 0 & 2\beta_1 + 2\beta_2 & 0 & \dots & 0 \\ 0 & 0 & -\alpha_2 & 0 & 2\alpha_1 + 2\alpha_2 & \dots & 0 \\ \vdots & & & & & \ddots & \\ 0 & 0 & 0 & \dots & & 2\alpha_1 + \alpha_2 & 0 \\ 0 & 0 & 0 & \dots & & 0 & 2\beta_1 + \beta_2 \end{bmatrix} \quad (3)$$

$$Q' = \begin{bmatrix}
\theta_1+\theta_2 & 0 & -2\theta_2 & 0 & \theta_2 & 0 & \cdots & \cdots & \cdots & \cdots & \cdots & \cdots & 0 \\
0 & \lambda_1+\lambda_2 & 0 & -2\lambda_2 & 0 & \lambda_2 & & & & & & & \\
-2\theta_2 & 0 & \theta_1+5\theta_2 & 0 & -4\theta_2 & 0 & & & & & & & \\
0 & -2\lambda_2 & 0 & \lambda_1+5\lambda_2 & 0 & -4\lambda_2 & 0 & & & & & & \\
\theta_2 & 0 & -4\theta_2 & 0 & \theta_1+6\theta_2 & 0 & & 0 & & & & & \\
0 & \lambda_2 & 0 & -4\lambda_2 & 0 & \lambda_1+6\lambda_2 & 0 & & 0 & & & & \\
& & & & & & 0 & \theta_1+6\theta_2 & 0 & -4\theta_2 & 0 & \theta_2 & 0 \\
& & & & & & & 0 & \lambda_1+6\lambda_2 & 0 & -4\lambda_2 & 0 & \lambda_2 \\
& & & & & & & -4\theta_2 & 0 & \theta_1+5\theta_2 & 0 & -2\theta_2 & 0 \\
& & & & & & & & -4\lambda_2 & 0 & \lambda_1+5\lambda_2 & 0 & -2\lambda_2 \\
& & & & & & & \theta_2 & & -2\theta_2 & 0 & \theta_1+\theta_2 & 0 \\
0 & \cdots & \cdots & \cdots & \cdots & \cdots & \cdots & 0 & \lambda_2 & 0 & -2\lambda_2 & 0 & \lambda_1+\lambda_2
\end{bmatrix} \qquad (4)$$

$$Q'' = \begin{bmatrix}
5\theta_1+\theta_2 & 0 & -2\theta_2 & 0 & \theta_2 & 0 & \cdots & \cdots & \cdots & \cdots & \cdots & \cdots & 0 \\
0 & 5\lambda_1+\lambda_2 & 0 & -2\lambda_2 & 0 & \lambda_2 & & & & & & & \\
-2\theta_2 & 0 & 5\theta_1+5\theta_2 & 0 & -4\theta_2 & 0 & & & & & & & \\
0 & -2\lambda_2 & 0 & 5\lambda_1+5\lambda_2 & 0 & -4\lambda_2 & 0 & & & & & & \\
\theta_2 & 0 & -4\theta_2 & 0 & 5\theta_1+6\theta_2 & 0 & & 0 & & & & & \\
0 & \lambda_2 & 0 & -4\lambda_2 & 0 & 5\lambda_1+6\lambda_2 & 0 & & 0 & & & & \\
& & & & & & 0 & 5\theta_1+6\theta_2 & 0 & -4\theta_2 & 0 & \theta_2 & 0 \\
& & & & & & & 0 & 5\lambda_1+6\lambda_2 & 0 & -4\lambda_2 & 0 & \lambda_2 \\
& & & & & & & -4\theta_2 & 0 & 5\theta_1+5\theta_2 & 0 & -2\theta_2 & 0 \\
& & & & & & & & -4\lambda_2 & 0 & 5\lambda_1+5\lambda_2 & 0 & -2\lambda_2 \\
& & & & & & & \theta_2 & & -2\theta_2 & 0 & 5\theta_1+\theta_2 & 0 \\
0 & \cdots & \cdots & \cdots & \cdots & \cdots & \cdots & 0 & \lambda_2 & 0 & -2\lambda_2 & 0 & 5\lambda_1+\lambda_2
\end{bmatrix}$$
$$(5)$$

$$S' = \begin{bmatrix}
6\theta_1 + \theta_2 & 0 & -2\theta_2 & 0 & \theta_2 & 0 & \cdots & \cdots & \cdots & \cdots & \cdots & \cdots & 0 \\
0 & 6\lambda_1 + \lambda_2 & 0 & -2\lambda_2 & 0 & \lambda_2 & \ddots & \ddots & \ddots & \ddots & \ddots & \ddots & \vdots \\
-2\theta_2 & 0 & 6\theta_1 + 5\theta_2 & 0 & -4\theta_2 & 0 & \ddots & & & & & & \vdots \\
0 & -2\lambda_2 & 0 & 6\lambda_1 + 5\lambda_2 & 0 & -4\lambda_2 & 0 & \ddots & & & & & \vdots \\
\theta_2 & 0 & -4\theta_2 & 0 & 6\theta_1 + 6\theta_2 & 0 & \ddots & 0 & \ddots & & & & \vdots \\
0 & \lambda_2 & 0 & -4\lambda_2 & 0 & 6\lambda_1 + 6\lambda_2 & 0 & \ddots & 0 & \ddots & & & \vdots \\
\vdots & \ddots & \ddots & \ddots & \ddots & \ddots & \ddots & \ddots & & \ddots & & & \vdots \\
\vdots & \ddots & \ddots & \ddots & \ddots & \ddots & \ddots & 0 & 6\theta_1 + 6\theta_2 & 0 & -4\theta_2 & 0 & \theta_2 & 0 \\
\vdots & \ddots & \ddots & \ddots & \ddots & \ddots & \ddots & & 0 & 6\lambda_1 + 6\lambda_2 & 0 & -4\lambda_2 & 0 & \lambda_2 \\
\vdots & \ddots & \ddots & \ddots & \ddots & \ddots & \ddots & & -4\theta_2 & 0 & 6\theta_1 + 5\theta_2 & 0 & -2\theta_2 & 0 \\
\vdots & \ddots & \ddots & \ddots & \ddots & \ddots & \ddots & & & -4\lambda_2 & 0 & 6\lambda_1 + 5\lambda_2 & 0 & -2\lambda_2 \\
\vdots & \ddots & \ddots & \ddots & \ddots & \ddots & \ddots & & \theta_2 & \ddots & -2\theta_2 & 0 & 6\theta_1 + \theta_2 & 0 \\
0 & \cdots & \cdots & \cdots & \cdots & \cdots & \cdots & 0 & \lambda_2 & 0 & -2\lambda_2 & 0 & 6\lambda_1 + \lambda_2
\end{bmatrix} \tag{6}$$

II. RESULTS

Axial strain images obtained by GLUE using high regularization parameter values have been reported in Fig. 1. For the four-layer simulated data, the continuity weights have been set to 15 times the optimal values. For the other datasets, 10 times stronger parameter sets than the optimal ones have been used. It is evident that high continuity weights reduce the estimation variance at the cost of visual contrast and edge sharpness.

Fig. 2 shows SOUL strain images for the soft-inclusion simulation dataset using optimal and 50% stronger regularization parameter values. It is evident that except slight loss of target-background contrast, a moderate increment of continuity weights has no visual effect on the strain image quality.

Fig. 3 demonstrates the effect of γ on TDE. The strain plots for one RF line of the simulated uniform phantom show that the top few samples exhibit incorrect TDE when the first sample is not regularized. GLUE also suffers from this issue since it does not regularize the top sample. Fig. 3 shows that SOUL resolves this issue by imposing a first-order continuity constraint on the first sample of an RF line.

Fig. 4 shows the effect of pixel size on continuity parameter values. In this experiment, the four-layer simulated phantom has been upsampled by a factor of 2. SOUL strain images obtained from this upsampled phantom using regular and 50% lower continuity weights have been reported. Both sets of parameters generate high-quality strain images. The effect of upsampling on the strain image corresponding to regular weights is negligible. On the other hand, lower level of regularization slightly increases the estimation variance.

The strain images for Realizations 2 and 3 for the simulated layer phantom are shown in Fig. 5. Hybrid and GLUE exhibit extensive strain variability, whereas MPWC-Net++ fails to obtain the true strain values in deep tissue regions. SOUL outperforms the other techniques by producing low-variance strain maps with high contrast among different tissue layers.

Lateral strain images obtained by GLUE and SOUL from the experimental breast phantom have been shown in Fig. 6. Due to lower resolution of ultrasound in the lateral direction, the lateral strain images are not as good as the axial counterpart. However, it is visually evident that SOUL substantially outperforms GLUE. This observation is clearer in Fig. 7 where the lateral strain images for liver Patient 2 have been shown. GLUE fails to distinguish the tumor from healthy tissue whereas SOUL successfully reveals the tumorous region.

(a) Simulated layer phantom (b) Soft-inclusion simulated phantom (c) Breast phantom (d) Liver Patient 1 (e) Liver Patient 2
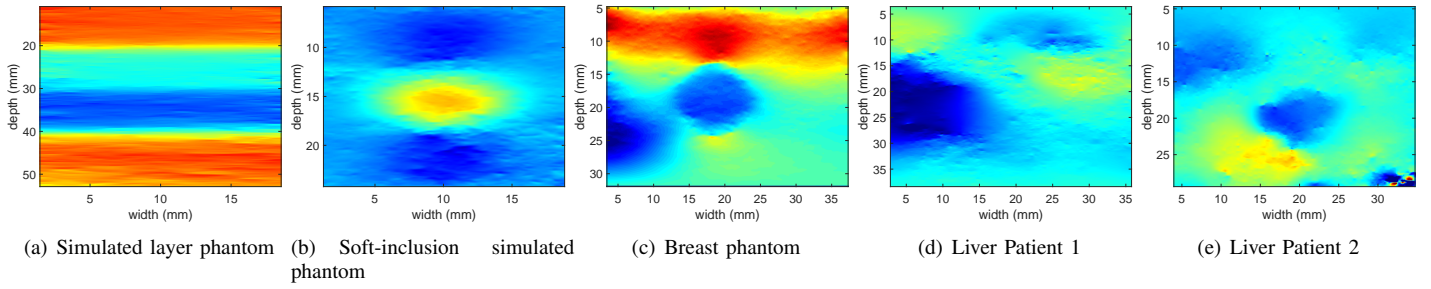
Fig. 1: GLUE strain images with strong regularization. Columns 1 to 5 show the strain images for four-layer simulated phantom, soft-inclusion simulated phantom, breast phantom, liver Patients 1 and 2, respectively.
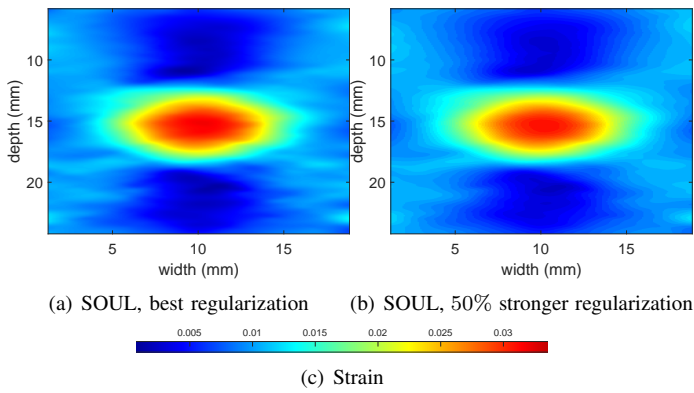

(a) SOUL, best regularization (b) SOUL, 50% stronger regularization

(c) Strain

Fig. 2: Axial strain images obtained from the soft-inclusion simulation phantom. Columns 1 and 2 depict strain images from SOUL with optimal and 50% stronger regularization weights, respectively.

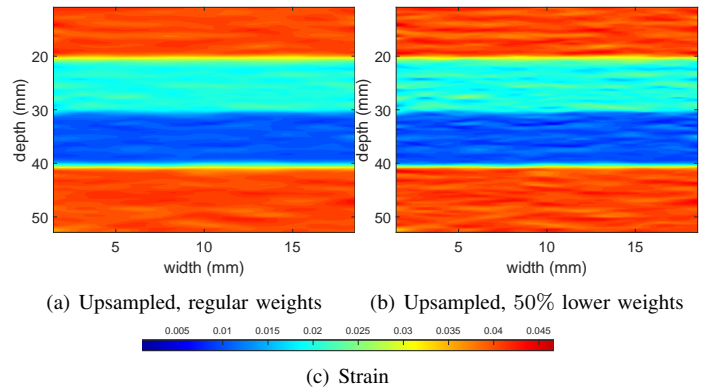(a) Upsampled, regular weights (b) Upsampled, 50% lower weights

(c) Strain

Fig. 4: Axial strain images obtained from the upsampled four-layer phantom using SOUL. Columns 1 and 2 represent strain images with regular and 50% lower continuity weights, respectively.
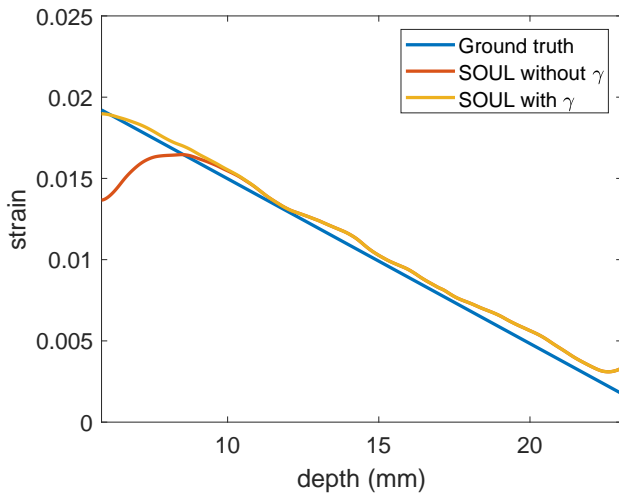

Fig. 3: Strain plots for the simulated uniform phantom.

(a) Hybrid, 2   (b) GLUE, 2   (c) MPWC-Net++, 2   (d) SOUL, 2

(e) Hybrid, 3   (f) GLUE, 3   (g) MPWC-Net++, 3   (h) SOUL, 3
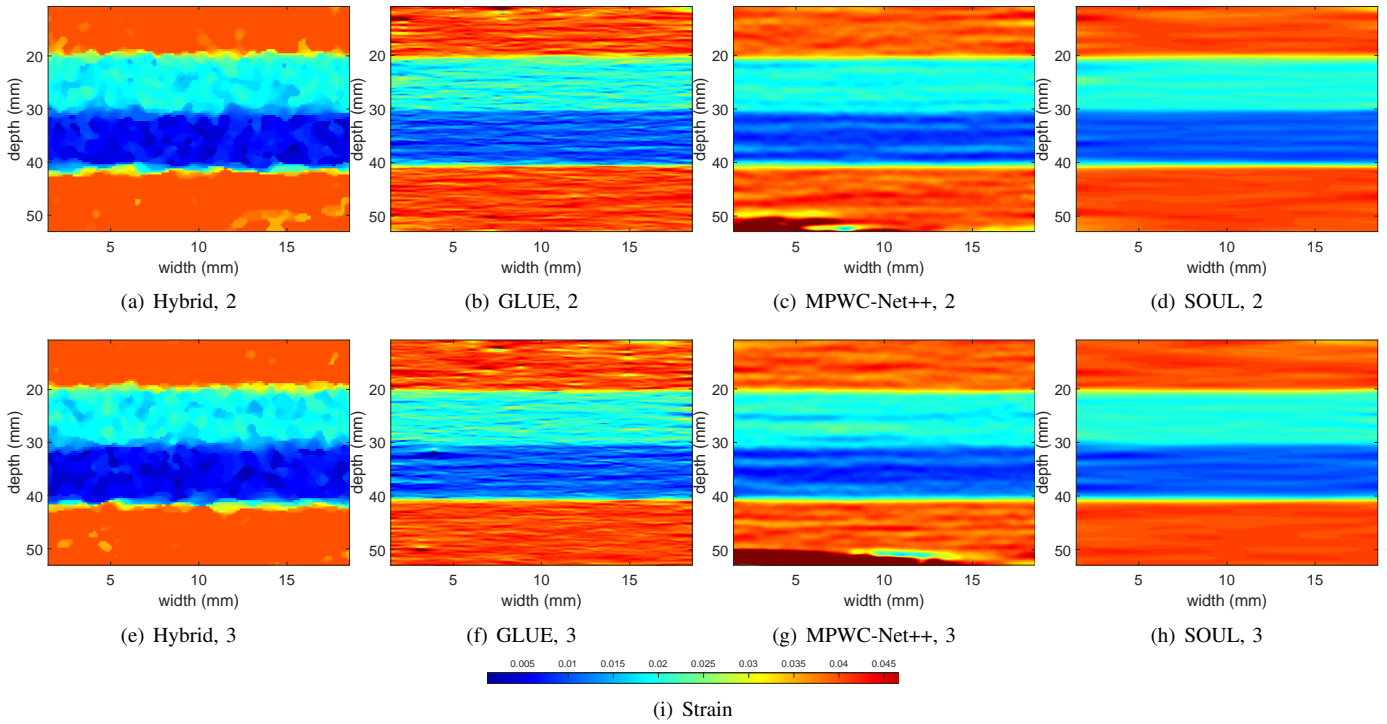
(i) Strain

Fig. 5: Results obtained from the simulated layer phantom with different realizations of scatterer position and amplitude. Columns 1 to 4 show the strain images produced by Hybrid, GLUE, MPWC-Net++ and SOUL, respectively. Rows 1 and 2 correspond to Realizations 2 and 3, respectively.
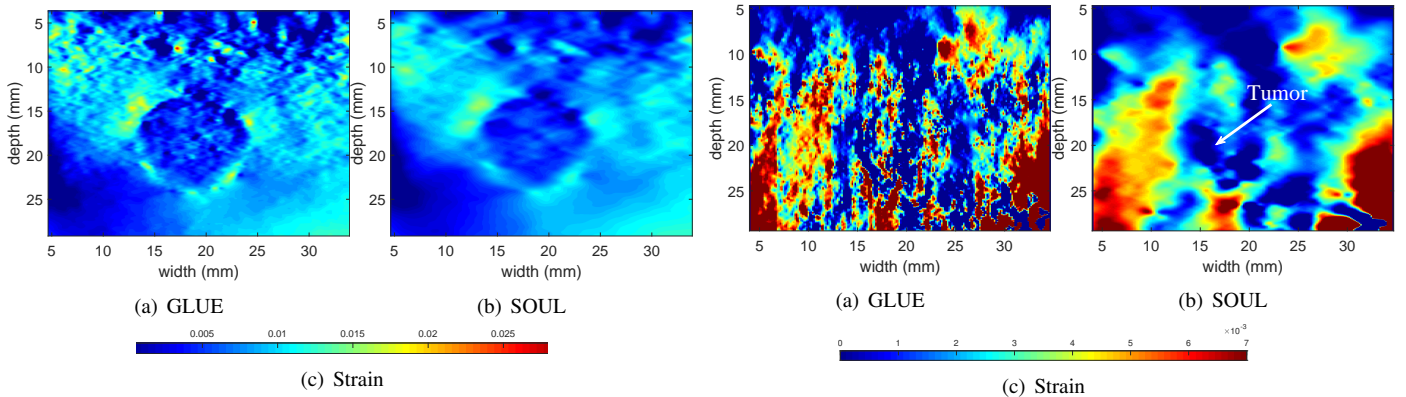

(a) GLUE   (b) SOUL

(c) Strain

Fig. 6: Lateral strain images obtained from the experimental phantom. Columns 1 and 2 correspond to GLUE and SOUL, respectively.

(a) GLUE   (b) SOUL

(c) Strain

Fig. 7: Lateral strain results obtained from liver Patient 2. Columns 1 and 2 represent GLUE and SOUL strain images, respectively.